Molecular Motions and Hydrogen-Bonding Networks in (o-Aminoanilinium)–(Crown Ethers)–[PMo$_{12}$O$_{40}$]$^{4-}$ Crystals

Daigoro Endo,[1] **Tomoyuki Akutagawa,**[*2] **Kazuya Kubo,**[1,3] **Shin-ichiro Noro,**[1,3]
Leroy Cronin,[4] **and Takayoshi Nakamura**[*1,3]

[1]Graduate School of Environmental Earth Science, Hokkaido University, N10W5, Kita-ku, Sapporo, Hokkaido 060-0810

[2]Institute of Multidisciplinary Research for Advanced Materials (IMRAM), Tohoku University,
2-1-1 Katahira, Aoba-ku, Sendai, Miyagi 980-8577

[3]Research Institute for Electronic Science, Hokkaido University, N20W10, Kita-ku, Sapporo, Hokkaido 001-0020

[4]WestCHEM, Department of Chemistry, University of Glasgow, Glasgow G12 8QQ, U. K.

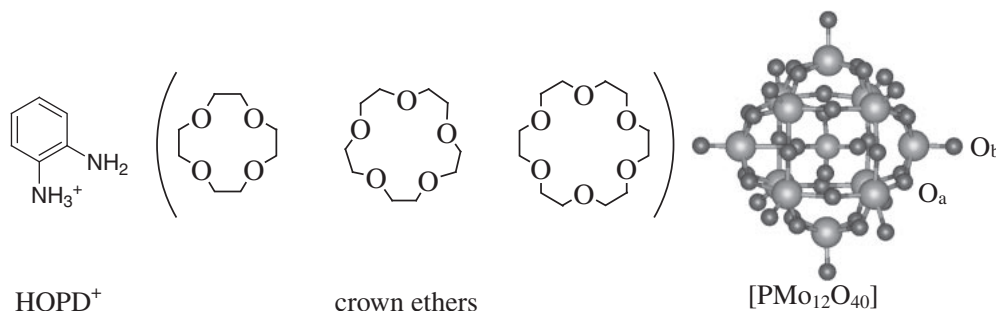Received November 28, 2011; E-mail: tnaka@es.hokudai.ac.jp

Single crystals formed from hydrogen-bonding supramolecular cations of o-aminoanilinium (HOPD$^+$)–crown ethers, (HOPD$^+$)([12]crown-4), (HOPD$^+$)([15]crown-5), and (HOPD$^+$)([18]crown-6), and one-electron-reduced [PMo$_{12}$O$_{40}$]$^{4-}$ Keggin-type clusters were synthesized. The crystal structures and dielectric responses of the three new compounds (HOPD$^+$)$_4$([12]crown-4)$_4$[PMo$_{12}$O$_{40}$]$^{4-}$·4CH$_3$CN (**1**), (HOPD$^+$)$_4$([15]crown-5)$_4$[PMo$_{12}$O$_{40}$]$^{4-}$ (**2**), and (HOPD$^+$)$_4$([18]crown-6)$_4$[PMo$_{12}$O$_{40}$]$^{4-}$·8CH$_3$CN (**3**) were examined. The CH$_3$CN molecules in salts **1** and **3** were included in zero-dimensional pores and one-dimensional channels, respectively; higher thermal stability was observed in the former lattice because of its extended hydrogen-bonding network. Large frequency- and temperature-dependent dielectric responses were confirmed in salts **2** and **3**, whereas the dielectric response of salt **1** was quite small. The fixed orientation of HOPD$^+$ because of the hydrogen-bonding network was consistent with the dielectric property of salt **1**. In contrast, large magnitudes of dielectric responses in the temperature range above 280 K were observed for salt **3**. Thermal motions of CH$_3$CN molecules in the channel were the origin of such dielectric responses. In salt **2**, the thermally activated coupled motion of the orthogonally arranged HOPD$^+$ pair along the C–NH$_3$$^+$-axis with the potential energy barrier of ca. 80 kJ mol^{-1} resulted in large dielectric responses.

Studies of artificial molecular rotation systems have attracted much attention because they can mimic highly functional biological motors.[1,2] The ATPase existing in the thylakoid membrane of mitochondria is a well-known molecular motor in biological systems and converts ADP into ATP during unidirectional rotation using a proton gradient across the membrane.[1,2] Among a variety of artificial molecular rotators, unidirectional rotation of a molecule in solution was realized by utilizing shuttle-like molecular motion in a catenane derivative.[3,4] Unidirectional rotation was also achieved by photo- and thermal isomerization around a C=C bond.[4] Because the rotation in these compounds occurs in solution, the rotational directions are randomly distributed, although each molecule exhibited unidirectional rotation. To achieve bulk functionalities using molecular rotations, one promising approach is the use of crystalline rotator compounds, where each molecular rotator is precisely arranged in the crystal lattice according to the crystal symmetry.

Molecular rotations in the solid state have been typically observed in the plastic crystalline state, which has been called a rotator phase.[5] Spherically shaped molecules such as CCl$_4$, adamantane, and C$_{60}$ can form plastic crystalline states, in which the random molecular rotation around the center of gravity of each molecule takes place through thermal activation.[5,6] Although the developments of novel functionality arising from the molecular rotations in solids have attracted much attention, to the best of our knowledge, the molecular designs for such dynamic motion in crystalline states have been very limited.[7,8] One of the rare examples is the molecular gyroscope compounds extensively studied by Garcia-Garibay et al., in which the dielectric responses were discussed from the viewpoint of rotational dynamics.[8]

We have been studying the supramolecular rotators of (anilinium)(crown ether) assemblies in [Ni(dmit)$_2$] crystals (dmit^{2-}: 2-thione-1,3-dithiole-4,5-dithiolate).[9] The N–H$^+$···O hydrogen-bonding interaction between the ammonium moiety (–NH$_3$$^+$) of aniliniums and the oxygen atoms of crown ethers can form a variety of cationic supramolecular assemblies of (anilinium)(crown ether) in [Ni(dmit)$_2$] crystals. Among others, a twofold flip-flop motion of anilinium (Ani$^+$) and a threefold rotation of adamantylammonium (ADNH$_3$$^+$) along the C–NH$_3$$^+$-axis have been observed in single crystals of (Ani$^+$)([18]crown-6)[Ni(dmit)$_2$]$^-$ and (ADNH$_3$$^+$)([18]crown-6)[Ni(dmit)$_2$]$^-$, respectively; their molecular rotations were

Scheme 1. The molecular structures of *o*-aminoanilinium (HOPD$^+$), crown ethers ([12]crown-4, [15]crown-5, and [18]crown-6), and [PMo$_{12}$O$_{40}$]. The metal bridging Mo–O$_a$–Mo and terminal Mo=O$_b$ oxygen sites are shown in [PMo$_{12}$O$_{40}$].

confirmed by X-ray crystal structural analyses and solid-state NMR.[9b,9c] A useful design approach that realizes the bulk functionality of these crystals is the modification of the rotary unit. By replacing Ani$^+$ with *m*-fluoroanilinium (*m*-FAni$^+$) in the supramolecular cation, the twofold flip-flop motion of *m*-FAni$^+$ along the C–NH$_3$$^+$-axis in a (*m*-FAni$^+$)-(dibenzo[18]crown-6)[Ni(dmit)$_2$]$^-$ crystal caused a dipole inversion. The permanent dipole moment normal to the rotational axis introduced by fluorine substitution at the *m*-position of Ani$^+$ responded to the application of an outer electric field.[10] An order–disorder transition associated with the molecular rotation occurred at 348 K, which corresponded to a ferroelectric–paraelectric transition.[10] In addition to chemical designs using anilinium, the structural designs of crown ethers should also be an important methodology for obtaining rotational space within crystals. To construct a molecular rotator structure within closest-packed single crystals, it is important to make enough space for rotation of the aryl moiety of the anilinium derivatives that include the crown ether. (Anilinium)(crown ether) assemblies are useful structural building blocks because of their flexibility in chemical design. In (*m*-FAni$^+$)(dibenzo[18]crown-6)[Ni(dmit)$_2$]$^-$ crystals, the larger size of dibenzo[18]crown-6 compared with [18]crown-6 played an important role in realizing the rotation of *m*-FAni$^+$.[10]

For the counter anion of cationic supramolecular rotator structures, we have utilized [Ni(dmit)$_2$], which is known for its unique electric and magnetic properties such as superconductivity and ferromagnetic transitions.[11] The π-planar [Ni(dmit)$_2$]$^-$ anion has an open-shell electronic structure and has a tendency to form the π-dimer, as a one-dimensional array and/or a two-dimensional layer within the crystals through the π-stacking interaction and the lateral S⋯S contacts.[10–12] As a result, [Ni(dmit)$_2$] molecules tend to take a tight and closest-packing configuration in the crystal, which is not advantageous for reserving space for molecular rotation.[9]

In this paper, we focus on polyoxometalates (POMs) as counter anions of supramolecular rotator units.[13,14] A variety of POMs have been prepared by the condensation of corresponding [MO$_4$]$^{2-}$ (M = Mo, V, W, Nb, and others); their molecular structures depend on such synthesis conditions as reducing reagents and the pH of the solution.[13,14] Although the structural diversity of POMs ranges from [Mo$_6$O$_{19}$]$^{2-}$, [Mo$_8$O$_{26}$]$^{4-}$, [P$_2$Mo$_{18}$O$_{62}$]$^{6-}$, to gigantic ball-shaped [Mo$_{132}$O$_{372}$(CH$_3$COO)$_{30}$(H$_2$O)$_{72}$]$^{42-}$, ring-shaped [Mo$_{154}$O$_{462}$H$^+$$_{14}$(H$_2$O)$_{70}$]$^{14-}$, and so on,[15] one of the best-

known POMs is the spherical Keggin cluster of [PMo$_{12}$O$_{40}$]$^{3-}$. This anion is constructed from one central PO$_4$$^{3-}$ and 12 corner-sharing [MoO$_6$] octahedrons. It has a spherical molecular structure with a diameter of ca. 1 nm (Scheme 1). Yellow [PMo$_{12}$O$_{40}$]$^{3-}$ can be reduced to a black, one-electron-reduced [PMo$_{12}$O$_{40}$]$^{4-}$ state bearing one $S = 1/2$ spin on the Mo^V site within the cluster.[13] This $S = 1/2$ spin can move freely between the 12 Mo sites within the [PMo$_{12}$O$_{40}$]$^{4-}$ cluster at room temperature. An order–disorder transition occurs at ca. 40 K, in which the $S = 1/2$ spin becomes fixed on one Mo site. This was confirmed from the line-width change of the ESR spectra.[16] Both the spherical molecular shape and the spin state of the [PMo$_{12}$O$_{40}$]$^{4-}$ cluster have the potential to form novel molecular assemblies by combining with supramolecular cationic structures. [PMo$_{12}$O$_{40}$]$^{4-}$ is much larger than the π-planar [Ni(dmit)$_2$]$^-$ anion. In addition, with its spherical shape and a number of proton-accepting sites for hydrogen bonding, unique cation–anion arrangements can be expected that should be advantageous for the dynamic motion of supramolecular cations.

We have previously reported the crystal structures and magnetic properties of (*p*-phenylenediamine)–(crown ether)–[PMo$_{12}$O$_{40}$]$^{4-}$ salts, where the supramolecular cationic structures of (HPPD$^+$)([12]crown-4), (HPPD$^+$)([15]crown-5), or (HPPD$^+$)([18]crown-6) coexisted with [PMo$_{12}$O$_{40}$]$^{4-}$ (HPPD$^+$ is the monoprotonated species of *p*-phenylenediamine).[17] In this paper, we adopted *o*-phenylenediamine (OPD) to form cationic supramolecular structures with the crown ethers [12]crown-4, [15]crown-5, and [18]crown-6. The OPD molecule can accept one proton, forming a monoprotonated HOPD$^+$ cation, which formed N–H$^+$⋯O hydrogen-bonding (HOPD$^+$)-(crown ether) assemblies. The second amino group at the *o*-position of HOPD$^+$ introduces a dipole moment orthogonal to the C–NH$_3$$^+$ direction, which can respond to an external electric field. The amino group at the *o*-position is close enough to the crown ether to interact through hydrogen bonding. This interaction will also affect the molecular motion in the crystal. The HOPD$^+$ cation in (HOPD$^+$)(dibenzo[18]crown-6)-[Ni(dmit)$_2$]$^-$ crystals showed a thermal fluctuating pendulum motion, which was the origin of quite large dielectric responses at temperatures above 200 K in low-frequency measurements.[18] In the present study, we synthesized three single crystals: (HOPD$^+$)$_4$([12]crown-4)$_4$[PMo$_{12}$O$_{40}$]$^{4-}$·4CH$_3$CN (**1**), (HOPD$^+$)$_4$([15]crown-5)$_4$[PMo$_{12}$O$_{40}$]$^{4-}$ (**2**), and (HOPD$^+$)$_4$-([18]crown-6)$_4$[PMo$_{12}$O$_{40}$]$^{4-}$·8CH$_3$CN (**3**) (Scheme 1). The

Table 1. Selected Crystal Parameters of Salts **1**–**3**

	1	**2**	**2**	**2**	**2**	**3**
Temperature/K	90	173	223	273	323	90
Chemical formula	$C_{64}H_{112}O_{56}$-$N_{12}Mo_{12}P$	$C_{64}H_{116}O_{60}$-$N_8Mo_{12}P$	$C_{64}H_{116}O_{60}$-$N_8Mo_{12}P$	$C_{64}H_{116}O_{60}$-$N_8Mo_{12}P$	$C_{66}H_{116}O_{60}$-$N_8Mo_{12}P$	$C_{88}H_{156}O_{64}$-$N_{16}Mo_{12}P$
Formula weight	3127.89	3139.89	3139.89	3139.89	3139.89	3644.52
Space group	$P\bar{1}$ (#2)	$P\bar{1}$ (#2)	$P\bar{1}$ (#2)	$P\bar{1}$ (#2)	$P\bar{1}$ (#2)	$P\bar{1}$ (#2)
a/Å	13.559(3)	13.3034(5)	13.3576(7)	13.4142(5)	13.4860(6)	14.164(5)
b/Å	13.632(3)	14.5907(7)	14.6076(7)	14.6225(6)	14.6328(7)	17.301(7)
c/Å	15.595(4)	15.9004(7)	15.8995(9)	15.9193(6)	15.9345(8)	17.367(8)
α/degrees	105.591(9)	64.622(2)	64.630(2)	64.617(2)	64.582(2)	118.399(12)
β/degrees	112.471(9)	66.118(2)	66.113(2)	66.068(2)	66.024(2)	91.935(11)
γ/degrees	96.115(9)	67.991(2)	67.996(2)	67.949(2)	67.921(2)	112.768(10)
V/Å^3	2493.8(10)	2473.0(2)	2485.9(3)	2500.6(2)	2516.5(2)	3328(2)
Z	1	1	1	1	1	1
D_{calcd}/g cm^{-3}	2.083	2.108	2.113	2.085	2.072	1.819
μ/cm^{-1}	15.721	15.857	15.801	15.699	15.600	11.970
No. of refl. meas.	54353	24469	19914	24436	24618	32218
No. of indep. used	16954	11229	9022	11287	11348	15038
$\sigma(I)$	2.0	3.0	2.5	3.0	2.0	2.0
R[a]	0.1216	0.0773	0.0803	0.0704	0.0697	0.0586
$R_w(F^2)$[a]	0.1110	0.0724	0.0969	0.703	0.1078	0.1557
GOF	1.297	1.348	1.206	1.291	0.753	1.078

a) $R = \Sigma||F_o| - |F_c||/\Sigma|F_o|$ and $R_w = [\Sigma(\omega(F_o^2 - F_c^2)^2)/\Sigma\omega(F_o^2)^2]^{1/2}$.

systematic size change of the crown ethers from [12]crown-4, [15]crown-5, to [18]crown-6 affected the cation–anion arrangements and molecular motions of the supramolecular units in the crystals.

Experimental

Instruments, Materials, and Methods. Infrared (IR, 400–7600 cm^{-1}) spectra measurements were carried out on KBr disks using a Perkin-Elmer Spectrum 2000 spectrophotometer with a resolution of 4 cm^{-1}. UV–vis–NIR spectra (350–3200 nm) were measured on KBr disks using a Perkin-Elmer Lambda-19 spectrophotometer with a resolution of 8 nm. Elemental analyses of C, H, and N were measured using a Yanaco MT-6 CHN Recorder at the Hokkaido University instrumental analysis division equipment management center.

Commercially available *o*-phenylenediamine (OPD) and $H_3[PMo_{12}O_{40}]\cdot nH_2O$ ($n = 20$), purchased from Tokyo Kasei Inc., were used to grow the crystals without further purification. The crystals were grown using the standard diffusion method in an H-shaped cell ($\approx$50 mL). $(H^+)_3[PMo_{12}O_{40}]\cdot nH_2O$ ($\approx$100 mg) and OPD (50 mg) with the selected crown ether (150 mg) were introduced into opposite sides of the H-shaped cell, which was filled with CH_3CN (distilled prior to use). After one week, single crystals were obtained as black blocks. The stoichiometries of the salts **1**, **2**, and **3** were determined by X-ray structural analysis as $(HOPD^+)_4([12]crown-4)_4$-$[PMo_{12}O_{40}]^{4-}\cdot 4CH_3CN$ (**1**), $(HOPD^+)_4([15]crown-5)_4$-$[PMo_{12}O_{40}]^{4-}$ (**2**), and $(HOPD^+)_4([18]crown-6)_4[PMo_{12}O_{40}]^{4-}\cdot 8CH_3CN$ (**3**). Elemental analysis results are as follows. Salt **1**: Calcd for $C_{60}H_{106}O_{56}N_{10}PMo_{12}$: C, 23.66; H, 3.51; N, 4.60%. Found: C, 23.38; H, 3.55; N, 4.35%. Salt **2**: Calcd for $C_{64}H_{116}O_{60}N_8PMo_{12}$: C, 24.48; H, 3.72; N, 3.57%. Found: C, 24.57; H, 3.68; N, 3.74%. Salt **3**: Calcd for

$C_{76}H_{138}O_{64}N_{10}PMo_{12}$: C, 26.86; H, 4.09; N, 4.12%. Found: C, 26.01; H, 3.76; N, 4.28%. Because a portion of CH_3CN molecules already evaporated from the crystals **1** and **3** before the analysis, the number of CH_3CN molecules was adjusted according to the experimental results. The TG–DTA measurements were carried out using a Rigaku Thermo Plus TG8120 with a scanning rate of 5 K min^{-1} under N_2 flow. Because the weight loss was already seen even at room temperature, the number of solvent molecules in each unit cell could not be determined from TG data.

Crystallography. Crystallographic data (Table 1) were collected on a Rigaku Raxis-Rapid diffractometer using Mo Kα ($\lambda = 0.71073$ Å) radiation from a graphite monochromator. Structure refinements were performed using the full-matrix least-squares method on F^2. Calculations were performed using the CrystalStructure software packages.[19a] Parameters were refined using anisotropic temperature factors except for hydrogen atoms and the disordered [15]crown-5 molecules in salt **2**. The temperature-dependent X-ray structural analyses ($T = 173$, 233, 273, and 323 K) were examined for salt **2** to clarify the complicated conformational and orientational disorders. In salt **3**, guest MeCN molecules were highly disordered even at 90 K, therefore the SQUEEZE function of PLATON[19b] was used to eliminate the contribution of the electron density in the solvent region from the intensity data, and the solvent-free model was employed for the final refinement.

Crystallographic data have been deposited with Cambridge Crystallographic Data Centre: Deposition numbers CCDC 856049–856054. Copies of the data can be obtained free of charge via http://www.ccdc.cam.ac.uk/conts/retrieving.html (or from the Cambridge Crystallographic Data Centre, 12, Union Road, Cambridge, CB2 1EZ, U.K.; Fax: +44 1223 336033; e-mail: deposit@ccdc.cam.ac.uk).

Calculations. The relative energy of the model structures of salt **2** was calculated using the RHF/6-31(d) basis set.[20] The nearest-neighbor molecules around the HOPD$^+$ except for $[PMo_{12}O_{40}]^{4-}$ were included in the calculations of the potential energy curves. The model structures of salt **2** in the calculations were $(HOPD^+)_4([15]crown-5)_3$ (Figure 6). The atomic coordinates of salt **2** based on the X-ray crystal structural analysis at 223 K were used for the calculations. The geometry optimization of the disordered HOPD$^+$ structure and the conformation of [15]crown-5 were first carried out by empirical PM3 calculation. The relative energy of the model structures was obtained by evaluating the rigid rotation in the $C-NH_3^+$ direction. Rotations were performed at every 15° between orientations **I** and **II**, and the relative energies were calculated using fixed atomic coordinates.

Dielectric Measurements. Temperature-dependent dielectric constants were measured using the two-probe AC impedance method at the frequency of 100×10^3 Hz (HP4194A). A single crystal was placed in a cryogenic refrigerating system (Daikin PS24SS). The electrical contacts were prepared using gold paste (Tokuriki 8560) to attach the $10\,\mu m\phi$ gold wires to the single crystal.

Magnetic Susceptibility. The temperature-dependent magnetic susceptibility and the magnetization–magnetic field dependence were measured using a Quantum Design MPMS-XL5 SQUID magnetometer using polycrystalline samples. The applied magnetic field was 1 T for all temperature-dependent measurements.

Results and Discussion

Crystal Growth. The stoichiometries and protonated states of salts **1**–**3** were formulated as $(HOPD^+)_4([12]crown-4)_4$-$[PMo_{12}O_{40}]^{4-} \cdot 4CH_3CN$ (**1**), $(HOPD^+)_4([15]crown-5)_4$-$[PMo_{12}O_{40}]^{4-}$ (**2**), and $(HOPD^+)_4([18]crown-6)_4[PMo_{12}O_{40}]^{4-} \cdot 8CH_3CN$ (**3**), from X-ray crystal structural analysis. The changes in both protonated state from neutral OPD to monoprotonated HOPD$^+$ and in electronic state from $[PMo_{12}O_{40}]^{3-}$ to one-electron-reduced $[PMo_{12}O_{40}]^{4-}$ occurred during crystallization.[17,21] During the slow diffusion of the $(H^+)_3$-$[PMo_{12}O_{40}]^{3-}$ and OPD in CH₃CN over 2–3 days, the color of the mother liquor changed from yellow to violet–black, indicating the formation of one-electron-reduced mixed-valence $[PMo_{12}O_{40}]^{4-}$ species; then black single crystals of salts **1**–**3** were obtained. One-electron reduction to $[PMo_{12}O_{40}]^{4-}$ was achieved using the reducing reagent OPD; the oxidized OPD species were transformed to 2,3-diaminophenazine through a condensation reaction.[22]

Three-step acid dissociation constants of $pK_{a1} = 2.0$, $pK_{a2} = 3.6$, and $pK_{a3} = 5.3$ in acetone have been reported for $H_3[PMo_{12}O_{40}]$,[13,23] whereas the acid dissociation constants of H_2OPD^{2+} were $pK_{a1} = 1.30$ and $pK_{a2} = 4.47$ in H_2O.[24] The pK_{a1} of $(H^+)_3[PMo_{12}O_{40}]^{3-}$ is larger than that of diprotonated H_2OPD^{2+}, indicating the formation of monoprotonated HOPD$^+$ species in solution. The $N-H^+\cdots O$ hydrogen bonding between the HOPD$^+$ and [12]crown-4, [15]crown-5, and [18]crown-6 formed the $(HOPD^+)(crown ether)$ supramolecular cations, which were formed as single crystals with $[PMo_{12}O_{40}]^{4-}$. The monoprotonated species of HOPD$^+$ in the crystals were evaluated using vibrational spectra. The
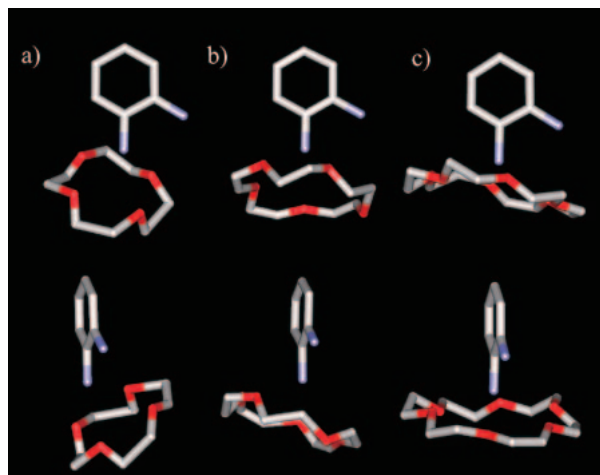

Figure 1. Supramolecular cation structures of a) (HOPD$^+$)-([12]crown-4) in salt **1** (**A**-unit at $T = 90$ K), b) (HOPD$^+$)-([15]crown-5) in salt **2** (**A**-unit at $T = 173$ K), and c) (HOPD$^+$)([18]crown-6) in salt **3** (**A**-unit at $T = 90$ K) viewed normal (upper figure) and parallel (lower figure) to the π-plane of the HOPD$^+$ cation. The conformational disorders of [15]crown-5 and hydrogen atoms are omitted in the figures. The **B**-units in salts **1**–**3** have slightly different conformations and were omitted to clarify the figures.

two characteristic absorption bands of N–H stretching at ≈ 3400 cm^{-1} and the N–H$^+$ band at ≈ 2900 cm^{-1} were assigned to the formation of monoprotonated HOPD$^+$ species in salts **1**–**3** (Figure S5).[25] The asymmetric C–O–C stretching modes of the corresponding crown ethers were also observed at around 1200 cm^{-1}.

The one-electron-reduced $[PMo_{12}O_{40}]^{4-}$ has one $S = 1/2$ spin on the cluster.[26] The temperature-dependent molar magnetic susceptibilities (T–χ_{mol}) of salts **1**–**3** were evaluated to confirm the electronic states of $[PMo_{12}O_{40}]^{4-}$ and their intercluster interactions in the crystals. The T–χ_{mol} plots of salts **1**–**3** showed paramagnetic behavior in the temperature range from 2 to 300 K, following the Curie–Weiss law (Figure S7).[27] The Curie constants of salts **1**, **2**, and **3** were 0.29, 0.35, and 0.32 emu K mol^{-1}, respectively, corresponding to the one $S = 1/2$ spin on the one-electron-reduced $[PMo_{12}O_{40}]^{4-}$ cluster. The intercluster interactions were small, as indicated by the magnitudes of the Weiss temperatures; 0.12, 0.13, and 0.11 K for salts **1**, **2**, and **3**, respectively.

Supramolecular Cationic Structures. The salts **1**–**3** had the same cation–anion formula of $(HOPD^+)(crown ether)$-$[PMo_{12}O_{40}]^{4-}$, where the size of the crown ether increased from [12]crown-4, to [15]crown-5, to [18]crown-6. Because the cavity diameters of [12]crown-4, [15]crown-5, and [18]crown-6 were 1.2–1.5, 1.7–2.5, and 2.6–3.2 Å, respectively, the $-NH_3^+$ of HOPD$^+$ just fitted in the cavity of [18]crown-6. Figure 1 summarizes the supramolecular cation structures of $(HOPD^+)([12]crown-4)$, $(HOPD^+)([15]crown-5)$, and $(HOPD^+)([18]crown-6)$ in salts **1**, **2**, and **3**, respectively. The conformation of the $(HOPD^+)(crown ether)$ assemblies was different for each salt. Table 2 summarizes selected structural parameters of the supramolecular cations in salts **1**–**3**.

Table 2. Selected Structural Parameters of (HOPD$^+$)(Crown Ethers) for the **A**- and **B**-Units in Salts **1**–**3**

	1	**2**[a]	**3**
Crown ethers	[12]crown-4	[15]crown-5	[18]crown-6
Cavity diameter/Å	1.2–1.5	1.7–2.5	2.6–3.2
Unit	**A, B**	**A, B**	**A, B**
d_{dv}/Å[b]	2.01, 1.95	1.56, 1.66	0.94, 0.92
d_{N-O}/Å[c]	2.80, 2.81	2.87, 2.93	2.93, 2.92
d'_{N-O}/Å[d]	3.19, 3.73	3.12, 3.56	3.19, 2.95
φ/deg[e]	54.8, 45.4	67.8, 59.1	89.9, 89.9

a) Structural parameter at $T = 173$ K. b) Deviation distance of the nitrogen atom from the mean oxygen plane of the crown ethers (d_{dv}). c) Average N–O distance between the nitrogen atom of –NH$_3^+$ and the oxygen atoms of the crown ethers. d) Average N–O distance between the nitrogen atom of –NH$_2$ at the *o*-position and the oxygen atoms of the crown ethers. e) Angle between the mean oxygen plane of the crown ether and the C6 plane of the HOPD$^+$ cation.

Two kinds of crystallographically independent (HOPD$^+$)-([12]crown-4), **A**-unit and **B**-unit, were observed in salt **1**. Because the cavity radius of [12]crown-4 was smaller than the ionic radius of –NH$_3^+$, the nitrogen atom of the ammonium moiety (–NH$_3^+$) in the HOPD$^+$ cation could not be tightly included by [12]crown-4. The average hydrogen-bonding N–O distances (d_{N-O}) between the –NH$_3^+$ of HOPD$^+$ and the four oxygen atoms of [12]crown-4 in the **A**- and **B**-units were 2.80 and 2.81 Å, respectively, which are nearly consistent with the standard hydrogen-bonding distance.[28] The deviation distance of the nitrogen atom from the mean O4 plane of [12]crown-4 (d_{dv}) was 2.01 and 1.95 Å, for the **A**- and **B**-units, respectively. The (HOPD$^+$)([12]crown-4) conformation was quite significantly different from the typical standup conformation of (Ani$^+$)([18]crown-6) and (*m*-FAni$^+$)([18]crown-6).[9,10] The π-plane of the HOPD$^+$ cation formed angles of 54.8 and 45.4° in the **A**- and **B**-units, respectively, with the O4 plane of [12]crown-4. The –NH$_2$ moieties at the *o*-position, which did not participate in the inclusion in the crown ethers, were also close to the O4 plane of [12]crown-4, with the N–O distance (d'_{N-O}) of the **A**- and **B**-units being 3.19 and 3.73 Å, respectively. The relatively short N–O distance in the **A**-unit suggests the formation of a hydrogen-bonding interaction.[28] This disorder was not observed in the (HOPD$^+$)([12]crown-4) structure at 90 K, suggesting a fixed cation conformation in salt **1**.

The (HOPD$^+$)([15]crown-5) supramolecule in salt **2** indicated quite complicated conformational and orientational disorders in both the HOPD$^+$ and [15]crown-5 (see the section on the Dynamic Properties of HOPD$^+$ in Salt **2**). In the crystal structural analyses at temperatures from 173 to 323 K, the conformational disorder of ethylene oxide (–CH$_2$–CH$_2$–O–) and orientational disorder were observed in [15]crown-5 and HOPD$^+$, respectively. Two kinds of crystallographically independent (HOPD$^+$)([15]crown-5) **A**- and **B**-units were observed in the unit cell of salt **2**. Because the cavity radius of [15]crown-5 was larger than that of [12]crown-4, the deviation distance of the nitrogen atom from the mean O5 plane of [15]crown-5 ($d_{dv} = 1.56$ and 1.66 Å for the **A**- and **B**-units, respectively) was 0.3–0.4 Å shorter than that for salt **1**.

The d_{N-O} between the –NH$_3^+$ and the oxygen atoms of [15]crown-5 in the **A**- and **B**-units were 2.87 and 2.93 Å, respectively ($T = 173$ K). The shortest distances between –NH$_2$ and [15]crown-5 in the **A**- and **B**-units were 3.12 and 3.56 Å, respectively, depending on the conformation of [15]crown-5. The angle between the mean O5 plane of [15]crown-5 and the C6 plane of HOPD$^+$ ($\varphi = 67.8$ and 59.1° for the **A**- and **B**-units, respectively) was larger than that of (HOPD$^+$)-([12]crown-4) in salt **1** ($\varphi = 54.8$ and 45.4°).

A typical standup conformation of (HOPD$^+$)([18]crown-6) was observed in salt **3** because of the size matching between the ionic radius of the ammonium moiety of HOPD$^+$ and the cavity radius of [18]crown-6. The d_{dv} values of 0.94 Å were about 0.6 Å smaller than those for salt **2** and similar to that in (NH$_4^+$)([18]crown-6).[29] The angle between the mean O6 plane of [18]crown-6 and the C6 plane of HOPD$^+$ ($\varphi = 90.0$°) indicated the standup conformation of the HOPD$^+$ cation with [18]crown-6, where the average hydrogen-bonding N–O distances between the nitrogen atom of HOPD$^+$ and the oxygen atoms of the crown ether were $d_{N-O} = 2.93$ and 2.92 Å for the **A**- and **B**-units, respectively. The d'_{N-O} was relatively small ($d'_{N-O} = 3.19$ and 2.95 Å for the **A**- and **B**-units, respectively), suggesting that both HOPD$^+$ cations were rather fixed through hydrogen bonding.

Crystal Structure. From the cation–anion formula of (HOPD$^+$)$_4$(crown ether)$_4$[PMo$_{12}$O$_{40}$]$^{4-}$ in salts **1**–**3**, a half unit of [PMo$_{12}$O$_{40}$] and two (HOPD$^+$)(crown ether) (**A**- and **B**-units) were the crystallographically independent structural units in salts **1**–**3**. The cation–anion packing structures in salts **1**–**3** were affected by the size of the (HOPD$^+$)(crown ether) supramolecule. In salts **1** and **3**, CH$_3$CN molecules filled the spaces formed through cation–anion arrangement in the crystal. Figure 2 summarizes the packing structures of salts **1**–**3**.

In salt **1**, [PMo$_{12}$O$_{40}$]$^{4-}$ clusters were surrounded by supramolecular cations, preventing intercluster interaction (Figure 2a). The HOPD$^+$ cations in the crystal are located close to the [PMo$_{12}$O$_{40}$]$^{4-}$ anions. Short distances between amino or ammonium moieties in HOPD$^+$ cations and the oxygen atoms of clusters (O$_b$ in Scheme 1) were observed. There are spaces between cation–anion arrangements, which were filled with CH$_3$CN molecules.

The intercluster interaction between [PMo$_{12}$O$_{40}$]$^{4-}$ anions was not observed in salt **2**, and the (HOPD$^+$)([15]crown-5) arrangement was different from that of salt **1**. Figure 2b shows the unit cell of salt **2** viewed along the *c* axis. Four (HOPD$^+$)([15]crown-5) supramolecular cations were assembled in the *ab* plane, and the assembly was elongated along the *c* axis. No CH$_3$CN molecules were included in the unit cell of salt **2**. The (HOPD$^+$)([15]crown-5) supramolecule may just fit for the closest-packing structure of the cation–anion arrangement. The cation–anion packing structure of salt **3** yielded a unique one-dimensional channel,[30] which was completely different from those of salts **1** and **2**. Figure 2c shows the unit cell viewed along the *c* axis, and the CPK representation of cation–anion arrangements within the *ab* plane, showing the formation of the channel structure in salt **3** (Figure 2d). From the TG–DTA diagram, the CH$_3$CN molecules in the channel were easily released from the crystal, even at 300 K.
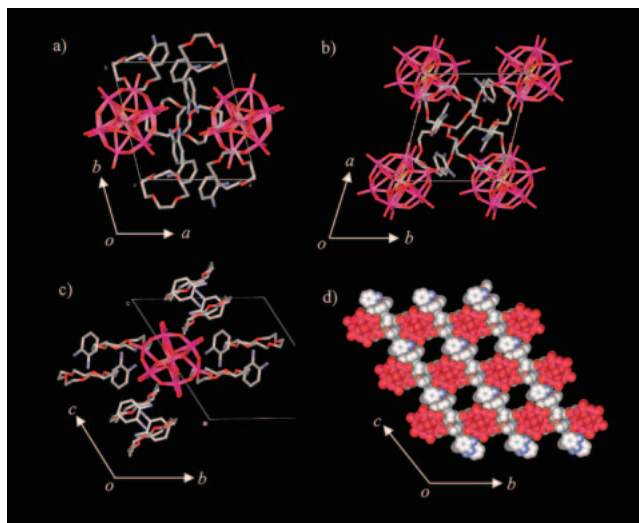
Figure 2. Packing structures of salts **1–3**. a), b) Unit cells of salts **1** and **2** viewed along the *c* axis. The orientational disorder of HOPD⁺ and conformational disorder of [15]crown-5 in salt **2** were omitted in the figure. c) Unit cell of salt **3** viewed along the *a* axis. d) CPK representation of the one-dimensional channel structure along the *a* axis of salt **3**. CH₃CN molecules filled the channel; they were omitted from the figure.

Cation Arrangements and Cation–Anion Interactions. The dipole moment of the HOPD⁺ cation arising from the amino group at the *o*-position caused a dipole–dipole interaction in the supramolecular cation arrangement. Figure 3 shows the supramolecular cation arrangement in salt **1**. Both the **A**-unit and **B**-unit formed dimers related by the inversion center (Figure 3a). Two HOPD⁺ cations in the **B**- and **B′**-units interacted strongly through the dipole–dipole interaction, whereas the two HOPD⁺ cations in the **A**- and **A′**-units sandwiched the two [12]crown-4 molecules. Although the one-dimensional array of **A–A′** and **B–B′** units was elongated along the $-b + c$ axis in the order –**A–A′**–**B–B′**–, intermolecular interactions between the **A–A′** and **B–B′** units were not observed along the $-b + c$ axis (Figure 3b).

The HOPD⁺ cations (**A**- and **B**-units) in salt **1** were located close to the $[PMo_{12}O_{40}]^{4-}$ anions. The shortest hydrogen-bonding distance (d_1 in Figure 3c) between the amino (–NH₂) moiety in the HOPD⁺ **A**-unit and the oxygen atoms of the clusters (Oᵦ oxygen in Scheme 1) was observed as $d_1 = 2.946(9)$ Å, and that (d_2 in Figure 3c) between the ammonium (–NH₃⁺) moiety of HOPD⁺ in the **A**-unit and the oxygen atoms of clusters (Oᵦ oxygen in Scheme 1) was observed as $d_2 = 2.983(6)$ Å ($T = 90$ K). The hydrogen-bonding interactions of d_1 and d_2 connected each $[PMo_{12}O_{40}]^{4-}$ cluster along the *a* axis. In contrast, the shortest hydrogen-bonding distance (d_3 in Figure 3c) between the amino (–NH₂) moiety of HOPD⁺ in the **B**-unit and the oxygen atoms of clusters (Oᵦ oxygen in Scheme 1) was observed as $d_3 = 2.877(6)$ Å, and that (d_4 in Figure 3c) between the ammonium (–NH₃⁺) moiety in HOPD⁺ **B**-unit and the oxygen atoms of clusters was observed as $d_4 = 3.1845(6)$ Å ($T = 90$ K). The d_3 and d_4 interactions connected each anion along the $a + c$ axis. A two-dimensional network between HOPD⁺ and $[PMo_{12}O_{40}]^{4-}$ through hydrogen
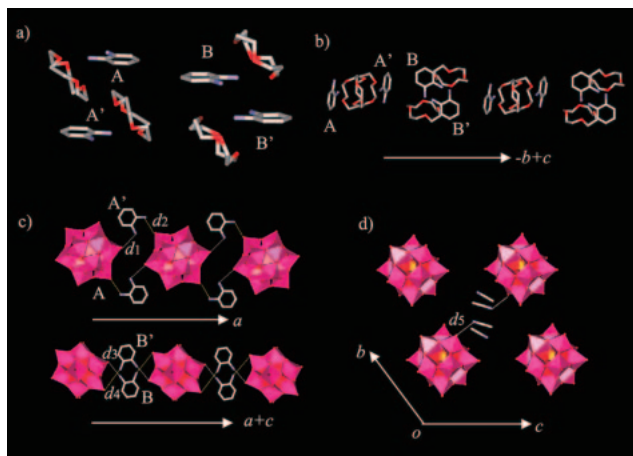

Figure 3. Supramolecular cation arrangements and cation–anion hydrogen-bonding interactions in salt **1** ($T = 90$ K). a) (HOPD⁺)([12]crown-4) **A**- and **B**-units viewed parallel to the π-plane of the HOPD⁺ cation. b) One-dimensional array of (HOPD⁺)([12]crown-4) **A**- and **B**-units along the $-b + c$ axis in the order –(**A–A′**)–(**B–B′**)–. c) Two-dimensional $[PMo_{12}O_{40}]^{4-}$ sheet through the hydrogen-bonding interactions between HOPD⁺ (**A**- and **B**-units) and oxygen atoms of the anion. The one-dimensional interaction between the **A**-unit and the $[PMo_{12}O_{40}]^{4-}$ anion was elongated along the *a* axis; the units further interacted through the one-dimensional interaction between the **B**-unit and $[PMo_{12}O_{40}]^{4-}$ anion along the $a + c$ axis. d) Hydrogen-bonding interactions between the nitrogen in the CH₃CN and the oxygen atom in $[PMo_{12}O_{40}]^{4-}$ unit.

bonding was observed in salt **1**. There are spaces between the hydrogen-bonding cation–anion arrangements, which were filled with CH₃CN molecules. Four CH₃CN molecules were located in the zero-dimensional crystalline pore. Two CH₃CN molecules in the unit cell interacted with $[PMo_{12}O_{40}]^{4-}$ cluster through hydrogen bonding ($d_5 = 3.123$ Å). In the TG measurement, the weight loss already began at room temperature in addition to a sharp decrease of 2.7% (two molar equivalents of CH₃CN) at 400 K with increasing temperature (Figure S9). The latter should correspond to the hydrogen-bonding CH₃CN within the pore. Structural change upon heating was examined using XRD measurements (Figure S8). Because the diffraction pattern after heating to 420 K was almost unchanged from that of the pristine sample, the crystal structure of **1** appeared to be relatively stable against the loss of solvent molecules upon heating because of the close packing of the molecules through the hydrogen-bonding network.

The shortest N–O distance between $[PMo_{12}O_{40}]^{4-}$ and the –NH₂ or –NH₃⁺ groups of the HOPD⁺ cation was greater than 3.50 Å at 173 K, which formed enough crystalline space for the dynamic motion of HOPD⁺ cations (see the section on Dynamics Properties of HOPD⁺ in Salt **2**).

Figure 4 shows the (HOPD⁺)([18]crown-6) arrangements in salt **3**. The supramolecular cations of the **A**- and **B**-units were arranged along the $b + c$ axis. The cation **A–A′** and **B–B′** pairs were related by the inversion center, and the dimer units of **A–A′** and **B–B′** were arranged along the $b + c$ axis. Around the HOPD⁺ cation, the neighboring [18]crown-6 molecules
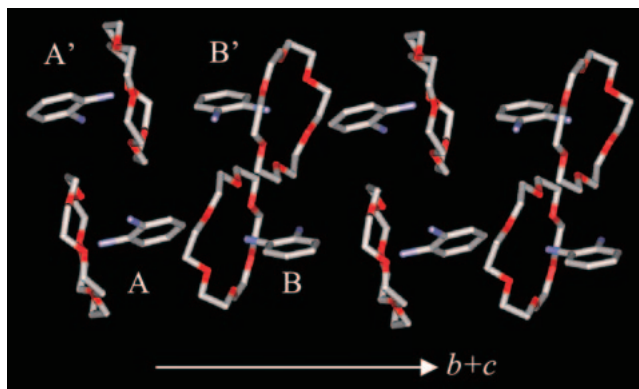
Figure 4. Supramolecular cation arrangement of (HOPD$^+$)-([18]crown-6) in salt **3**. Two kinds of crystallographically independent (HOPD$^+$)([18]crown-6) units, the **A**- and **B**-units were observed along the $b + c$ axis. The **A**–**A′** and **B**–**B′** pairs were related by the inversion center.

Figure 5. Supramolecular cation structure of (HOPD$^+$)-([15]crown-5) and cation arrangement in salt **2**. a) (HOPD$^+$)([15]crown-5) **A**-unit viewed normal to the π-plane of HOPD$^+$. The conformational disorder of [15]crown-5 was omitted in the figure. b), c) (HOPD$^+$)-([15]crown-5) **B**-unit viewed normal and parallel, respectively, to the C–NH$_3^+$-axis of HOPD$^+$. Two kinds of orientational disorders were observed in the HOPD$^+$ cation of orientations **I** (blue) and **II** (red). d), e) The supramolecular cation arrangements along the c axis. The **A**, **A′**, **B**, and **B′** units were arranged along the c axis.

restricted the rotation of the HOPD$^+$ cation along the C–NH$_3^+$-axis by the large steric hindrance between the amino group of HOPD$^+$ and the ethylene units of [18]crown-6. The cation–anion packing structure of salt **3** yielded a unique one-dimensional channel,[29] which was completely different from those of salts **1** and **2**. Figure 2d shows the unit cell viewed along the a axis, and the CPK representation of the cation–anion arrangements within the bc plane. A channel structure with the cross-sectional area of $8.5 \times 6.0\,\text{Å}^2$ was formed along the b axis, and was filled with CH$_3$CN molecules. The shortest N–O distance between the HOPD$^+$ **A**-unit and the [PMo$_{12}$O$_{40}$]$^{4-}$ anion was 3.26 Å, indicating the formation of weak hydrogen-bonding interactions. The HOPD$^+$ **B**-unit was almost isolated, with the shortest N–O distance being greater than 4 Å, and the intercluster interaction was also small because of the long P–P distance of 14.4 Å between the neighboring [PMo$_{12}$O$_{40}$]$^{4-}$ clusters along the a axis.

From the TG–DTA diagram (Figure S9), the CH$_3$CN molecules in the channel were easily released from the crystal, even at 300 K. The crystals readily decomposed upon exposure to the atmosphere. The XRD pattern of the sample after heating at 390 K was different from that of the pristine sample (Figure S8, indicating that the crystal structure of salt **3** was unstable upon the loss of CH$_3$CN molecules from the channel. The magnitude of the hydrogen-bonding interaction in salt **3** was weaker than those of salt **1**, which reflected the thermal stability of these two compounds).

Dynamic Properties of HOPD$^+$ in Salt 2. Figure 5 summarizes the supramolecular cation structures of (HOPD$^+$)-([15]crown-5) and its arrangements in salt **2**. To evaluate the dynamic properties of the supramolecular cations, temperature-dependent X-ray crystal structural analyses at 173, 223, 273, and 323 K were performed. Rather complicated orientational and conformational disorders were observed in the HOPD$^+$ cation and [15]crown-5, respectively, in the temperature range from 173 to 323 K. The conformational disorder of the ethylene oxide (–O–CH$_2$–CH$_2$–) moiety in [15]crown-5 was observed in both **A**- and **B**-units throughout the temperature range. The HOPD$^+$ cation in the **A**-unit was at a fixed position, whereas an orientational disorder of the HOPD$^+$ cation was observed in
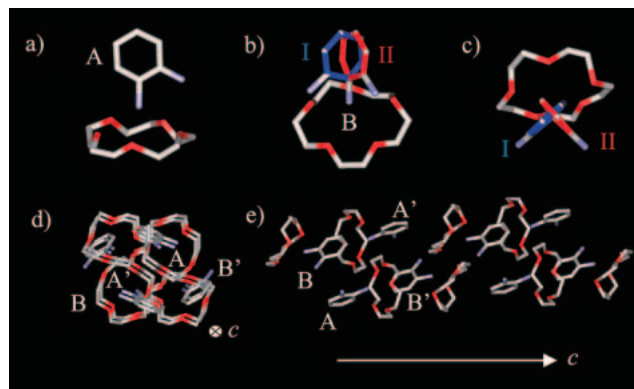
the **B**-unit. Two HOPD$^+$ orientations **I** and **II** (indicated by red and blue, respectively, in Figures 5b and 5c) shearing the C–NH$_3^+$-axis existed, which were observed as an average structure in the X-ray crystal structural analysis. Although the thermal motion of the (HOPD$^+$)([15]crown-5) supramolecule was enhanced by increasing the temperature, no drastic conformational change of the **A**- and **B**-units was observed at temperatures up to 323 K. The C6 plane of HOPD$^+$ in orientation **I** was orthogonal to that in orientation **II**, and the occupancy factors for orientations **I** and **II** were equal to each other (1:1) at 173 K. The same orthogonal orientation and occupancy factors were observed in the crystal structural analyses at 223, 273, and 323 K. The supramolecular cation **A**- and **B**-units were arranged along the c axis (Figure 5d and Figure 5e). Four (HOPD$^+$)([15]crown-5) units of **A**–**B**–**A′**–**B′** were arranged within the ab plane, which was elongated along the c axis. The one-dimensional tetramer arrangements of (HOPD$^+$)([15]crown-5) were isolated from each other, and were surrounded by [PMo$_{12}$O$_{40}$]$^{4-}$ anions.

No evidence of flip-flop motion of HOPD$^+$ was observed in the **A**-unit in the temperature-dependent X-ray crystal structural analyses, indicating the fixed HOPD$^+$ orientation in the crystal. Thermal parameters of HOPD$^+$ and [15]crown-5 increased with increasing temperature. The molecular motions of the supramolecular cation were essentially thermally activated. As it is difficult to distinguish dynamic orientational disorders of HOPD$^+$ cations from static ones, we estimated the possible orientations from the potential energy calculation for the rotation of HOPD$^+$ around the C–NH$_3^+$-axis.

In the crystal structure, the one (HOPD$^+$)([15]crown-5) **B**-unit was surrounded by two neighboring **A**-units, one disordered HOPD$^+$ **B**-unit (Figure 5), and [PMo$_{12}$O$_{40}$]$^{4-}$ clusters. Two disordered **B**-units give four kinds of relative orientations of HOPD$^+$, (**I**–**I′**), (**I**–**II′**), (**II**–**I′**), and (**II**–**II′**), where the prime
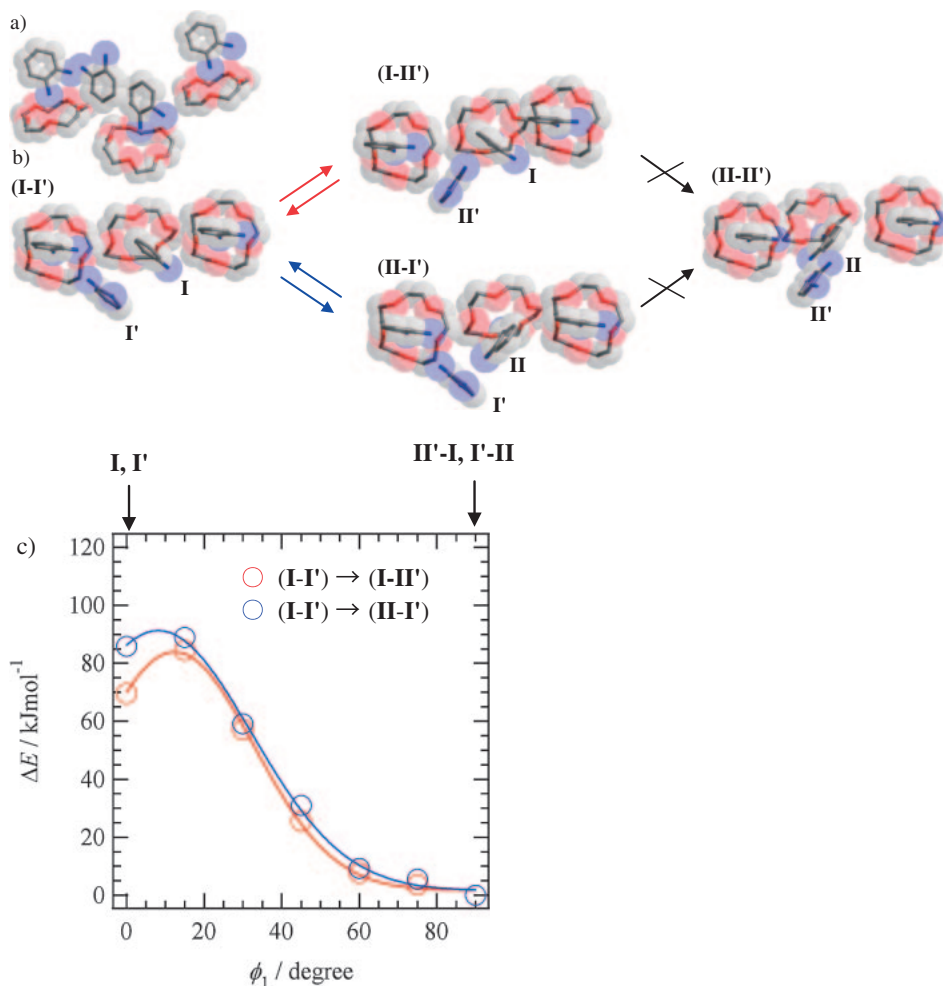
Figure 6. Molecular motions of orthogonally disordered HOPD$^+$ cations (**B**-unit) in salt **2**. a) The calculated structure of (HOPD$^+$)$_4$([15]crown-5)$_3$ in salt **2**. b) The combination of two HOPD$^+$ orientations (**I** and **II**), which were observed in the orthogonal disorder in the **B**-unit. The three kinds of HOPD$^+$ orientations of (**I–I′**), (**I–II′**), and (**II–I′**) pairs were considered for the calculations of the potential energy curves. The prime symbol indicates the neighboring HOPD$^+$ molecule corresponding to the original atomic coordinate (**I** and **II**). c) Potential energy (ΔE) vs. rotation angle ϕ_1 plots for (**I–I′**)–(**I–II′**) (red circles) and (**I–I′**)–(**II–I′**) (blue circles) around the C–NH$_3$$^+$ bond. The bule and red lines are guides for the eyes.

symbol indicates the neighboring molecule corresponding to the original atomic coordinate (**I** and **II**). We discuss the potential energy curves from orientation **I** ($\phi_1 = 0°$) to **II** ($\phi_1 = 90°$), because further rotation was obviously impossible given the large steric hindrance from neighboring [PMo$_{12}$O$_{40}$]$^{4-}$ anions. For this reason, the [PMo$_{12}$O$_{40}$]$^{4-}$ anion was removed from the calculations for simplicity.

The single-point energies of the model structure of (HOPD$^+$)$_4$([15]crown-5)$_3$ were calculated using the RHF/6-31(d) basis set,[23] where the relative energy (ΔE) was plotted against the rotational angle (ϕ_1) of the HOPD$^+$ cation along the C–NH$_3$$^+$-axis. Because the original orientation **I** (blue) and **II** (red) of the HOPD$^+$ **B**-unit was observed in the orthogonal arrangements (Figures 5b and 5c), the potential energy curves from orientation **I** ($\phi_1 = 0°$) to **II** ($\phi_1 = 90°$) were evaluated as possible molecular motions in salt **2**. According to the restricted rotation from orientation **I** to **II**, four kinds of representative HOPD$^+$ arrangements from (**I–I′**), (**I–II′**), (**II–I′**), to (**II–II′**) were considered as the ideal HOPD$^+$ arrangements in salt **2**. The (**I–I′**) and (**II–I′**) orientations were adopted for the parallel

arrangements of two HOPD$^+$ cations (Figure 6b). However, the two HOPD$^+$ cations in the (**II–II′**) orientation existed at quite close positions, where two neighboring hydrogen atoms were bonded to each other. Therefore, the calculations from (**I–II′**) or (**II–I′**) to (**II–II′**) were not carried out. When the (**I–I′**) orientation was realized in salt **2**, the twofold orientational disorder of the amino group in HOPD$^+$ should have been observed in the X-ray crystal structural analysis, but no such disorder was observed in the structural analysis of the (**I–I′**) orientation. Therefore, the (**I–I′**) orientation should be a metastable or unstable state, which was consistent with the potential calculations. To explain the orthogonal disorder of the HOPD$^+$ cation in the **B**-unit, the (**I–II′**) and (**II–I′**) orientations were reasonable HOPD$^+$ cation arrangements. The potential energy curves for the rotation of HOPD$^+$ from (**I–I′**) at $\phi_1 = 0°$ to (**I–II′**) and/or (**II–I′**) at $\phi_1 = 90°$ orientations are shown in Figure 6c.

Both the (**I–II′**) and (**II–I′**) orientations were consistent with the orthogonal disorder of HOPD$^+$ in the **B**-unit of X-ray crystal structural analysis. Starting from the (**I–I′**) orientation, the (**I–II′**) orientation was obtained by the rotation of HOPD$^+$ (**I′**)
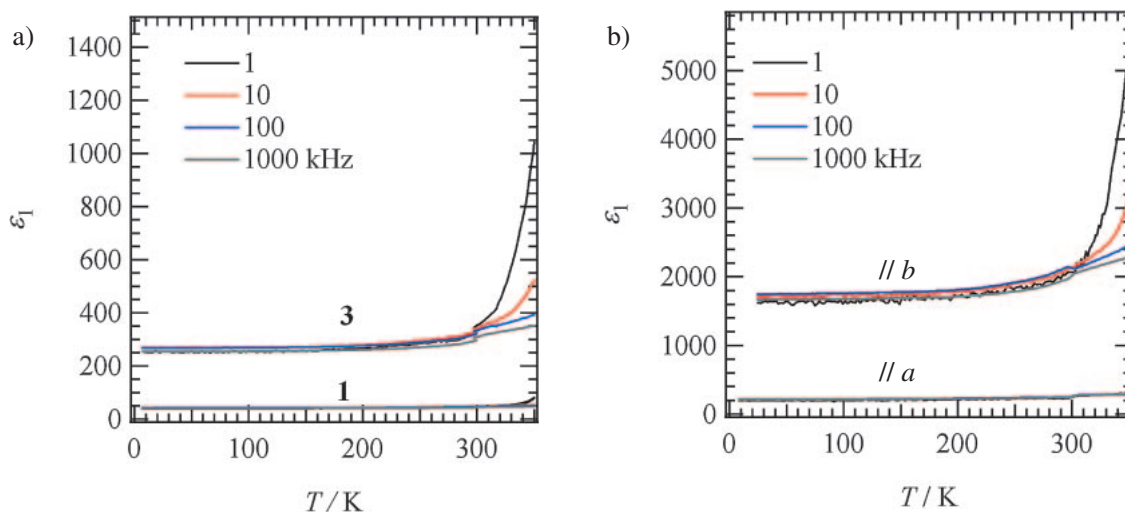
Figure 7. Temperature-dependent dielectric constants (ε_1) of a) single crystals of salts **1** and **3**, and b) anisotropic ε_1 of a single crystal of salt **2**. The electric field was applied perpendicular to the C–NH$_3$$^+$-axis of the HOPD$^+$ cations.

with the fixed orientation of HOPD$^+$ (**I**). Figure 6c shows the potential energy (ΔE)–rotation angle ϕ_1 plots from (**I–I′**) to (**I–II′**) (red circles) and from (**I–I′**) to (**II–I′**) (blue circles) for every 15° of rotation. The ΔE value of $\approx 80\,\mathrm{kJ\,mol^{-1}}$ at $\phi_1 = 0°$, indicating a metastable or unstable state of the (**I–I′**) orientation, decreased gradually to $\Delta E \approx 0\,\mathrm{kJ\,mol^{-1}}$ around $\phi_1 = 90°$, resulting in the stable (**I–II′**) orientation. Almost the same ΔE–ϕ_1 plot was observed for the potential energy curve from the (**I–I′**) to (**II–I′**) orientation. Both orientations (**I–II′**) and (**II–I′**) became the most stable orientations following the same potential energy curves. Because the energy difference between the most stable orthogonal (**I–II′**) and/or (**II–I′**) orientations and the parallel (**I–I′**) one was $\approx 100\,\mathrm{kJ\,mol^{-1}}$, the orientational conversion from (**I–II′**) to (**II–I′**) can be thermally activated through the transition state of parallel orientation of the (**I–I′**) state. Because the interconversion of two HOPD$^+$ orientations occurred in the HOPD$^+$ pair, the coupled orthogonal motion of the HOPD$^+$ pair is one of the possible dynamic motions in salt **2**. Such thermal motion yielded the thermal fluctuation of HOPD$^+$ cations, resulting in their dipole fluctuations.

Dielectric Responses. The frequency- and temperature-dependent dielectric constants (ε_1) of single crystals **1**–**3** were examined to evaluate the dynamic properties of the crystals.[5b,31] In dielectric spectroscopy, thermal motions of polar units in the measurement frequency range from 1 to 1000 kHz were observed in the frequency and temperature responses. The symmetric molecules of [12]crown-4, [18]crown-6, and [PMo$_{12}$O$_{40}$] are insensitive to the dielectric response, whereas the thermal motions of the polar units of HOPD$^+$ and CH$_3$CN molecules largely contributed to the dielectric responses.

Figure 7a shows the ε_1–T plots of single crystals **1** and **3** measured parallel to the π-plane of the HOPD$^+$ cation. The crystal structures of salts **1** and **3** did not show orientational disorder in the (HOPD$^+$)([12]crown-4) and (HOPD$^+$)- ([18]crown-6) supramolecules at 90 K. Neither frequency dependence nor temperature dependence of ε_1 were observed in salt **1** (Figure 7a), which was consistent with the crystal structure. Because the CH$_3$CN molecules in zero-dimensional pores have high thermal stability around room temperature,

the polar CH$_3$CN molecules did not contribute much to the dielectric response, even at 350 K. In contrast, a large dielectric response at temperatures above 300 K was observed in the ε_1–T plots of salt **3**, although the orientational disorder was not observed in the (HOPD$^+$)([18]crown-6) at 90 K. Because the aryl rings of HOPD$^+$ were fixed to [18]crown-6 with relatively strong hydrogen-bonding interactions in addition to the steric hindrance from the neighboring [18]crown-6, the rotations of aryl rings were restricted in crystalline **3**. The large ε_1 response may originate from dynamic disorder of the crystal solvent. However, further examination was not possible because the room-temperature crystal structure was unavailable after the decomposition of the crystals at higher temperatures.

Figure 7b shows the anisotropic dielectric constants of a single crystal of salt **2** along the a and b axes; these directions correspond to the parallel and normal to the π-plane of the HOPD$^+$ cation. The dielectric response along the a axis was much smaller than that along the b axis. Because the b axis corresponded to the direction normal to the C–NH$_3$$^+$-axis of the orthogonally disordered HOPD$^+$ (**B**-unit), thermally activated motion of the HOPD$^+$ pair was observed as a relatively large dielectric response of salt **2**. The low-frequency dielectric enhancement corresponded to the slow molecular motion of the HOPD$^+$ pair within the crystal.

Conclusion

Different sizes of *o*-aminoanilinium (HOPD$^+$)(crown ether) assemblies of (HOPD$^+$)([12]crown-4), (HOPD$^+$)([15]crown-5), and (HOPD$^+$)([18]crown-6) were introduced into the one-electron-reduced [PMo$_{12}$O$_{40}$]$^{4-}$ as structurally flexible counter cations. The crystal structures of the three new compounds (HOPD$^+$)$_4$([12]crown-4)$_4$[PMo$_{12}$O$_{40}$]$^{4-}$·4CH$_3$CN (**1**), (HOPD$^+$)$_4$([15]crown-5)$_4$[PMo$_{12}$O$_{40}$]$^{4-}$ (**2**), and (HOPD$^+$)$_4$- ([18]crown-6)$_4$[PMo$_{12}$O$_{40}$]$^{4-}$·8CH$_3$CN (**3**) were examined from the viewpoints of crystal design and molecular motions. The size and conformation of the (HOPD$^+$)(crown ether) assemblies were modified according to the size of the crown ethers, which also affected the cation–anion arrangements and the dynamic properties of the supramolecules. CH$_3$CN

molecules existed in salts **1** and **3**, whereas the (HOPD$^+$)-([15]crown-5) supramolecule just fitted to form the closest cation–anion packing in salt **2**. In crystal **1**, a two-dimensional hydrogen-bonding network between [PMo$_{12}$O$_{40}$]$^{4-}$ and HOPD$^+$ formed a stable cation–anion framework with a pore structure. The CH$_3$CN molecules in the zero-dimensional pore of salt **1** showed high thermal stability, and the framework was preserved after losing CH$_3$CN by heating. On the other hand, the hydrogen-bonding network restricted the rotation of HOPD$^+$ in the supramolecular units, and no large dielectric response was observed. Because the hydrogen-bonding network did not extend over the whole crystal **3**, the channel structure of the cation–anion arrangement was thermally unstable and was decomposed by losing CH$_3$CN on heating. Relatively strong hydrogen bonding between the –NH$_2$ group of HOPD$^+$ and [18]crown-6 restricted HOPD$^+$ rotation. The CH$_3$CN molecules in the one-dimensional channel of salt **3** indicated the thermally activated motion with increasing temperature, which was the origin of large dielectric responses at low frequencies. Orientational disorder of HOPD$^+$ cations and conformational disorder of [15]crown-5 were observed in salt **2** by X-ray analysis at all measurement temperatures. Relatively large dielectric responses of salt **2** were observed at temperatures above 280 K, which were associated with the coupled orthogonal motion of HOPD$^+$ pairs with the potential energy barrier of $\approx$80 kJ mol^{-1}. The interconversion between the two orthogonal orientations of HOPD$^+$ pairs resulted in fluctuation of the dipole moment introduced by the *o*-amino substituent, which responded to the outer electric field.

Supporting Information

Atomic numbering scheme of structural analyses of salts **1**–**3**, IR, UV–vis–NIR spectra, temperature-dependent magnetic susceptibilities, and TG data. These materials are available free of charge on the web at http://www.csj.jp/journals/bcsj/.

References

1 L. Stryer, *Biochemistry*, Freeman, New York, **1995**.
2 a) T. Funatsu, Y. Harada, M. Tokunaga, K. Saito, T. Yanagida, *Nature* **1995**, *374*, 555. b) K. Kitamura, M. Tokunaga, A. H. Iwane, T. Yanagida, *Nature* **1999**, *397*, 129.
3 See for example: a) V. Balzani, A. Credi, F. M. Raymo, J. F. Stoddart, *Angew. Chem., Int. Ed.* **2000**, *39*, 3348. b) G. S. Kottas, L. I. Clarke, D. Horinek, J. Michl, *Chem. Rev.* **2005**, *105*, 1281. c) E. R. Kay, D. A. Leigh, F. Zerbetto, *Angew. Chem., Int. Ed.* **2007**, *46*, 72.
4 a) T. R. Kelly, H. De Silva, R. A. Silva, *Nature* **1999**, *401*, 150. b) N. Koumura, R. W. J. Zijlstra, R. A. van Delden, N. Harada, B. L. Feringa, *Nature* **1999**, *401*, 152. c) T. R. Kelly, R. A. Silva, H. De Silva, S. Jasmin, Y. Zhao, *J. Am. Chem. Soc.* **2000**, *122*, 6935. d) B. L. Feringa, *Acc. Chem. Res.* **2001**, *34*, 504. e) N. Koumura, E. M. Geertsema, M. B. van Gelder, A. Meetsma, B. L. Feringa, *J. Am. Chem. Soc.* **2002**, *124*, 5037. f) R. A. van Delden, N. Koumura, N. Harada, B. L. Feringa, *Proc. Natl. Acad. Sci.*

U.S.A. **2002**, *99*, 4945. g) B. L. Feringa, R. A. van Delden, M. K. J. ter Wiel, *Pure Appl. Chem.* **2003**, *75*, 563. h) D. A. Leigh, J. K. Y. Wong, F. Dehez, F. Zerbetto, *Nature* **2003**, *424*, 174. i) R. A. van Delden, J. H. Hurenkamp, B. L. Feringa, *Chem.—Eur. J.* **2003**, *9*, 2845.
5 a) J. N. Sherwood, *The Plastically Crystalline State: Orientationally Disordered Crystals*, John Wiley & Sons, Chichester, **1979**. b) W. C. Hamilton, J. A. Ibers, *Hydrogen Bonding in Solid: Methods of Molecular Structure Determination*, W. A. Benjamin Inc., New York, **1968**. c) N. G. Parsonage, L. A. K. Staveley, *Disorder in Crystals*, Oxford University Press, Oxford, **1978**.
6 R. D. Johnson, C. S. Yannoni, H. C. Dorn, J. R. Salem, D. S. Bethune, *Science* **1992**, *255*, 1235.
7 a) T. Akutagawa, T. Motokizawa, K. Matsuura, S. Nishihara, S.-i. Noro, T. Nakamura, *J. Phys. Chem. B* **2006**, *110*, 5897. b) Q. Ye, T. Akutagawa, N. Hoshino, T. Kikuchi, S.-i. Noro, R.-G. Xiong, T. Nakamura, *Cryst. Growth Des.* **2011**, *11*, 4175.
8 See references in: a) M. A. Garcia-Garibay, *Proc. Natl. Acad. Sci. U.S.A.* **2005**, *102*, 10771. b) T.-A. V. Khuong, J. E. Nuñez, C. E. Godinez, M. A. Garcia-Garibay, *Acc. Chem. Res.* **2006**, *39*, 413.
9 a) T. Akutagawa, K. Shitagami, S. Nishihara, S. Takeda, T. Hasegawa, T. Nakamura, Y. Hosokoshi, K. Inoue, S. Ikeuchi, Y. Miyazaki, K. Saito, *J. Am. Chem. Soc.* **2005**, *127*, 4397. b) D. Sato, T. Akutagawa, S. Takeda, S.-i. Noro, T. Nakamura, *Inorg. Chem.* **2007**, *46*, 363. c) S. Nishihara, T. Akutagawa, D. Sato, S. Takeda, S.-i. Noro, T. Nakamura, *Chem.—Asian J.* **2007**, *2*, 1083. d) T. Akutagawa, T. Nakamura, *Dalton Trans.* **2008**, 6335.
10 T. Akutagawa, H. Koshinaka, D. Sato, S. Takeda, S.-I. Noro, H. Takahashi, R. Kumai, Y. Tokura, T. Nakamura, *Nat. Mater.* **2009**, *8*, 342.
11 P. Cassoux, L. Valade, H. Kobayashi, A. Kobayashi, R. A. Clark, A. E. Underhill, *Coord. Chem. Rev.* **1991**, *110*, 115.
12 a) J. M. Williams, J. R. Ferraro, R. J. Thorn, K. D. Carlson, U. Geiser, H. H. Wang, A. M. Kini, M.-H. Whangbo, in *Organic Superconductors: Synthesis, Structure, Properties, and Theory*, ed. by R. N. Grimes, Prentice-Hall, New Jersey, **1992**. b) T. Ishiguro, K. Yamaji, G. Saito, in *Organic Superconductors* in *Solid-State Sciences*, 2nd ed., ed. by M. Cardona, P. Fulde, K. von Klitzing, H.-J. Queisser, Springer-Verlag, Berlin, **1998**, Vol. 88.
13 a) *Polyoxometalate Molecular Science* in *NATO Science Series II. Mathematics, Physics and Chemistry*, ed. by J. J. Borrás-Almenar, E. Coronado, A. Müller, M. Pope, Kluwer Academic Publishers, London, **2001**, Vol. 98. b) *Polyoxometalate Chemistry: From Topology via Self-Assembly to Applications*, ed. by M. T. Pope, A. Müller, Kluwer Academic Publishers, London, **2001**. c) *Polyoxometalate Chemistry for Nano-Composite Design*, ed. by T. Yamase, M. T. Pope, Kluwer Academic Publishers, New York, **2002**. d) L. Cronin, in *From the Molecular to the Nanoscale: Synthesis, Structure, and Properties* in *Comprehensive Coordination Chemistry II*, Vol. 7, p. 1. doi:10.1016/B0-08-043748-6/06146-6.
14 a) A. Müller, P. Kögerler, C. Kuhlmann, *Chem. Commun.* **1997**, 1437. b) A. Müller, P. Kögerler, A. W. M. Dress, *Coord. Chem. Rev.* **2001**, *222*, 193. c) A. Müller, C. Serain, *Acc. Chem. Res.* **2000**, *33*, 2. d) A. Müller, S. Roy, *Coord. Chem. Rev.* **2003**, *245*, 153.
15 a) A. Müller, E. Krickemeyer, J. Meyer, H. Bögge, F. Peters, W. Plass, E. Diemann, S. Dillinger, F. Nonnenbruch, M. Randerath, C. Menke, *Angew. Chem., Int. Ed. Engl.* **1995**, *34*,

2122. b) A. Müller, S. K. Das, E. Krickemeyer, C. Kuhlmann, in *Inorganic Syntheses*, ed. by J. R. Shapley, Wiley, New York, **2004**, p. 191. c) A. Müller, S. K. Das, V. P. Fedin, E. Krickemeyer, C. Beugholt, H. Bögge, M. Schmidtmann, B. Hauptfleisch, *Z. Anorg. Chem.* **1999**, *625*, 1187. d) A. Müller, S. Q. N. Shah, H. Bögge, M. Schmidtmann, P. Kögerler, B. Hauptfleisch, S. Leiding, K. Wittler, *Angew. Chem., Int. Ed. Engl.* **2000**, *39*, 1614. e) A. Müller, S. Sarkar, S. Q. N. Shah, H. Bögge, M. Schmidtmann, S. Sarkar, P. Kögerler, B. Hauptfleisch, A. X. Trautwein, V. Schünemann, *Angew. Chem., Int. Ed. Engl.* **1999**, *38*, 3238. f) A. Müller, V. P. Fedin, C. Kuhlmann, H. Bögge, M. Schmidtmann, *Chem. Commun.* **1999**, 927.

16   a) R. A. Prados, P. T. Meiklejohn, M. T. Pope, *J. Am. Chem. Soc.* **1974**, *96*, 1261. b) R. A. Prados, M. T. Pope, *Inorg. Chem.* **1976**, *15*, 2547. c) C. Sanchez, J. Livage, J. P. Launay, M. Fournier, Y. Jeannin, *J. Am. Chem. Soc.* **1982**, *104*, 3194.

17   a) T. Akutagawa, D. Endo, H. Imai, S.-i. Noro, L. Cronin, T. Nakamura, *Inorg. Chem.* **2006**, *45*, 8628. b) T. Akutagawa, D. Endo, S.-i. Noro, L. Cronin, T. Nakamura, *Coord. Chem. Rev.* **2007**, *251*, 2547.

18   T. Akutagawa, H. Koshinaka, Q. Ye, S.-i. Noro, J. Kawamata, H. Yamaki, T. Nakamura, *Chem.—Asian J.* **2010**, *5*, 520.

19   a) *CrystalStructure*, ver. 3.6, Single crystal structure analysis software, **2004**, Rigaku Corporation and Molecular Structure Corporation. b) A. L. Spek, *J. Appl. Crystallogr.* **2003**, *36*, 7.

20   M. J. Frisch, G. W. Trucks, H. B. Schlegel, G. E. Scuseria, M. A. Robb, J. R. Cheeseman, J. A. Montgomery, Jr., T. Vreven, K. N. Kudin, J. C. Burant, J. M. Millam, S. S. Iyengar, J. Tomasi, V. Barone, B. Mennucci, M. Cossi, G. Scalmani, N. Rega, G. A. Petersson, H. Nakatsuji, M. Hada, M. Ehara, K. Toyota, R. Fukuda, J. Hasegawa, M. Ishida, T. Nakajima, Y. Honda, O. Kitao, H. Nakai, M. Klene, X. Li, J. E. Knox, H. P. Hratchian, J. B. Cross, C. Adamo, J. Jaramillo, R. Gomperts, R. E. Stratmann, O. Yazyev, A. J. Austin, R. Cammi, C. Pomelli, J. W. Ochterski, P. Y. Ayala, K. Morokuma, G. A. Voth, P. Salvador, J. J. Dannenberg, V. G. Zakrzewski, S. Dapprich, A. D. Daniels, M. C. Strain, O. Farkas, D. K. Malick, A. D. Rabuck, K. Raghavachari, J. B. Foresman, J. V. Ortiz, Q. Cui, A. G. Baboul, S. Clifford, J. Cioslowski, B. B. Stefanov, G. Liu, A. Liashenko, P. Piskorz, I. Komaromi, R. L. Martin, D. J. Fox, T. Keith, M. A. Al-Laham, C. Y. Peng, A. Nanayakkara, M. Challacombe, P. M. W. Gill, B. Johnson, W. Chen, M. W. Wong, C. Gonzalez, J. A. Pople, *Gaussian R03W*, Gaussian, Inc., Pittsburgh, PA, **2003**.

21   T. Akutagawa, F. Kudo, R. Tsunashima, S.-i. Noro, L. Cronin, T. Nakamura, *Inorg. Chem.* **2011**, *50*, 6711.

22   S. Upreti, A. Datta, A. Ramanan, *Cryst. Growth Des.* **2007**, *7*, 966.

23   I. V. Kozhevnikov, *Chem. Rev.* **1998**, *98*, 171.

24   *Handbook of Chemistry and Physics*, 83rd ed, CRC Press, New York, **2002**.

25   E. Akalin, S. Akyüz, *Vib. Spectrosc.* **2000**, *22*, 3.

26   a) L. Ouahab, M. Bencharif, A. Mhanni, D. Pelloquin, J.-F. Halet, O. Peña, J. Padiou, D. Grandjean, C. Garrigou-Lagrange, J. Amiell, P. Delhaes, *Chem. Mater.* **1992**, *4*, 666. b) C. J. Gómez-Garcia, L. Ouahab, C. Gimenez-Saiz, S. Triki, E. Coronado, P. Delhaès, *Angew. Chem., Int. Ed. Engl.* **1994**, *33*, 223. c) C. Bellitto, M. Bonamico, V. Fares, F. Federici, G. Righini, M. Kurmoo, P. Day, *Chem. Mater.* **1995**, *7*, 1475. d) E. Coronado, J. R. Galán-Mascarós, C. Giménez-Saiz, C. J. Gómez-García, S. Triki, *J. Am. Chem. Soc.* **1998**, *120*, 4671. e) E. Coronado, C. J. Gómez-García, *Chem. Rev.* **1998**, *98*, 273. f) M. Nyman, D. Ingersoll, S. Singh, F. Bonhomme, T. M. Alam, C. J. Brinker, M. A. Rodriguez, *Chem. Mater.* **2005**, *17*, 2885.

27   R. L. Carlin, *Magnetochemistry*, Springer-Verlag, Heidelberg, **1986**.

28   a) G. A. Jeffrey, in *An Introduction to Hydrogen Bonding*, ed. by D. G. Truhlar, Oxford University Press, New York, **1997**. b) T. Steiner, *Angew. Chem., Int. Ed.* **2002**, *41*, 48.

29   O. Nagano, A. Kobayashi, Y. Sasaki, *Bull. Chem. Soc. Jpn.* **1978**, *51*, 790.

30   a) S. Uchida, N. Mizuno, *Chem.—Eur. J.* **2003**, *9*, 5850. b) S. Uchida, N. Mizuno, *Coord. Chem. Rev.* **2007**, *251*, 2537. c) S. Uchida, R. Kawamoto, H. Tagami, Y. Nakagawa, N. Mizuno, *J. Am. Chem. Soc.* **2008**, *130*, 12370.

31   K. C. Kao, *Dielectric Phenomena in Solids*, Elsevier, Amsterdam, **2004**.